
Learning Unknown Interdependencies for Decentralized Root Cause Analysis in Nonlinear Dynamical Systems

Ayush Mohanty*

Paritosh Ramanan†

Nagi Gebraeel*

Abstract

Root cause analysis (RCA) in networked industrial systems, such as supply chains and power networks, is notoriously difficult due to unknown and dynamically evolving interdependencies among geographically distributed clients. These clients represent heterogeneous physical processes and industrial assets equipped with sensors that generate large volumes of *nonlinear*, high-dimensional, and heterogeneous IoT data. Classical RCA methods require partial or full knowledge of the system’s dependency graph, which is rarely available in these complex networks. While federated learning (FL) offers a natural framework for decentralized settings, most existing FL methods assume homogeneous feature spaces and retrainable client models. These assumptions are not compatible with our problem setting. Different clients have different data features and often run fixed, proprietary models that cannot be modified. This paper presents a federated cross-client interdependency learning methodology for feature-partitioned, nonlinear time-series data, without requiring access to raw sensor streams or modifying proprietary client models. Each proprietary local client model is augmented with a Machine Learning (ML) model that encodes cross-client interdependencies. These ML models are coordinated via a global server that enforces representation consistency while preserving privacy through calibrated differential privacy noise. RCA is performed using model residuals and anomaly flags. We establish theoretical convergence guarantees and validate our approach on extensive simulations and a real-world industrial cybersecurity dataset.

1 Introduction

Root-cause analysis (RCA) is a fundamental diagnostic method used to identify the underlying causes of system-level failures. RCA becomes significantly challenging in modern networked systems that are characterized by complex, and **often unknown**, interdependencies among geographically dispersed industrial assets (hereafter referred to as clients), such as smart cities [49], power networks [13, 4], and supply chains [55]. Characterizing these cross-client interdependencies is critical to mitigating the impacts of any disruptions and identifying their root causes.

Several conventional methods have been developed for learning interdependencies. They include Granger causality [17, 48], vector autoregression [16, 37], and structural equation modeling [24]. However, these methods assume that data from all the clients can be aggregated into a central server. In our industrial setting, this assumption breaks down. Clients generate large volumes of high-dimensional sensor data and are often governed by stringent data-sovereignty regulations. Therefore, centralized approaches for learning interdependencies are not adequate.

*School of Industrial and Systems Engineering, Georgia Institute of Technology, Atlanta, GA 30332

†School of Industrial Engineering and Management, Oklahoma State University, Stillwater, OK 74708

Limitations of existing decentralized methods. Federated learning (FL) [36] offers a promising alternative by enabling model training directly at the data source, thereby preserving privacy and minimizing communication overhead. In principle, FL provides a framework well-suited for distributed RCA: clients retain sensitive operational data locally while contributing to a shared model that can be used for RCA. However, there are unique challenges that limit the applicability of existing methods.

1. First, existing FL approaches that aim to capture directed dependencies (causality) [39, 14] are generally developed under the assumption of a homogeneous, shared feature space across clients (i.e., horizontal FL). This assumption is not applicable to our problem setting, where clients correspond to distinct processes or equipment types, each with unique sensors and feature representations. In such feature-partitioned (i.e., vertical FL) environments, cross-client causal modeling becomes substantially more challenging due to heterogeneous data features and site-specific temporal dynamics.
2. Second, our problem involves highly complex latent system-wide interactions that require discovering unknown, possibly causal, interdependencies directly from decentralized data [57, 3]. Unfortunately, federated graph learning formulations [51, 7] do not support this capability. For example, federated graph neural networks (FedGNNs) such as [19, 34, 38] rely on the availability of an explicit or partially observable adjacency matrix to encode the graph structure. This adjacency matrix typically reflects pre-defined relationships among clients, which are generally unknown in our problem setting.
3. Third, in many industrial settings, each client operates a proprietary model supplied by its original equipment manufacturer (OEM), which cannot be modified, retrained, or directly updated. Most state-of-the-art FL algorithms assume that client models are trainable and participate in federated parameter updates. However, this assumption fails in scenarios where model internals are inaccessible due to intellectual property constraints or certification requirements. Thus, learning must occur without altering the underlying client models. This poses a fundamental departure from prevailing FL paradigms.

Main Contributions: This paper proposes a federated framework that relies on collaboratively learning interdependencies across feature-partitioned OT clients. The key contributions are:

- We develop a novel federated cross-client interdependency learning algorithm that utilizes non-linear local ML models at each client to encode interdependency information communicated by an ML-based global server model. The local ML models are used to *augment* the representation generated by proprietary client models.
- Our framework enables decentralized RCA, where the server identifies the source of anomalies without direct access to client states or raw data. We propose that clients utilize the *residuals* from proprietary client models and their augmented forms to generate anomaly flags that identify the root cause (RC) and distinguish it from the propagated effect (PE).
- We provide theoretical guarantees that, under standard assumptions, our framework converges to the performance of a fully *centralized oracle*. Furthermore, to protect sensitive client data, we incorporate differential privacy into training and inference, where states and anomaly flags are perturbed with controlled noise, enabling secure communication.
- Extensive evaluations on synthetic datasets confirm the framework’s effectiveness in learning cross-client interdependencies, anomaly detection, and RCA performance. We also study the sensitivity to detection threshold and scalability in large systems. We further validate it on a real-world industrial testbed, demonstrating its effectiveness in learning interdependencies and performing decentralized RCA in an industrial control systems dataset.

2 Related Work

Anomaly Detection & Root Cause Analysis (RCA) in time-series: Multivariate time-series anomaly detection has been well-studied in centralized settings, addressing variable correlations [42, 15]. Decentralized approaches [30, 22, 12] improve scalability but fail to model interdependencies. Most anomaly detection methods omit RCA, limiting their mitigation utility. RCA typically uses centralized methods such as Granger causality [17, 48] and Vector Autoregression [32], which rely on raw data access. Recent RCA studies explore causal discovery and graphical models [40, 1, 9, 2, 25, 52, 43],

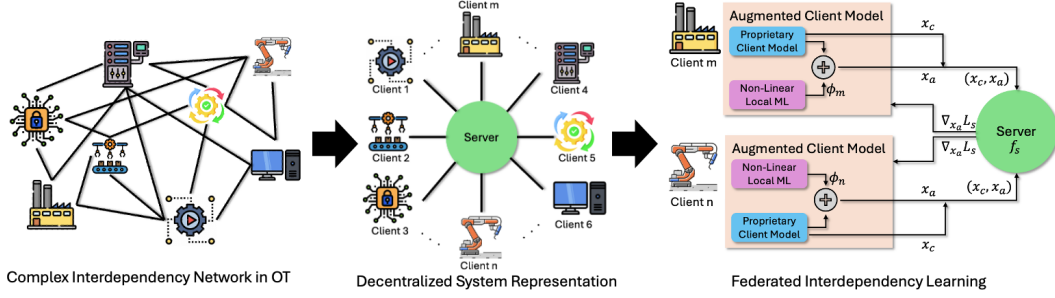


Figure 1: The proposed federated framework for learning interdependencies across OT clients

but a few such as [29, 28] address decentralization. Integrating decentralized RCA with anomaly detection, especially under unknown interdependencies, remains unexplored.

Vertical Federated Learning (VFL): Our approach aligns with VFL, where clients hold different features of the same sample; **in our case, features are time-series measurements, and samples correspond to timestamps.** Traditional VFL frameworks focus on classification tasks with fixed labels, which are either shared across clients [20, 21, 6], held by one client (called the “active client/party”) [11, 18, 56], or stored on servers [54, 5, 26]. With few exceptions, such as [10, 33], most studies use global models as simple aggregators rather than leveraging ML-based models, preventing them from learning interdependencies.

Related Domains: *Federated Multi Task Learning* [47, 35, 31, 8] focuses on parameter sharing in horizontally partitioned datasets, overlooking feature-based interdependency modeling. *Split Learning* [46, 41, 50] handles feature-based partitioning by splitting neural network layers but does not address anomaly detection or interdependencies.

3 Problem Setting

We consider a decentralized setup with M clients. Each client m observes **high-dimensional data** $y_m^t \in \mathbb{R}^{D_m}$ and uses a *proprietary client model* to compute its **lower-dimensional states** $(x_m^t)_c \in \mathbb{R}^{P_m}$ ($D_m \gg P_m$). Since these proprietary client models rely solely on locally available data y_m^t , it limits their ability to accurately capture cross-client interdependencies. To address this limitation, we use iterative optimization during training:

1. **Client.** Each client *augments* $(x_m^t)_c$ with a *non-linear ML* $\phi_m(y_m^t; \theta_m)$, producing $(x_m^t)_a$ where θ_m *locally encodes interdependencies*. Clients minimize a loss $(L_m)_a$ using both local $(\nabla_{\theta_m} (L_m)_a)$ and server-provided $(\nabla_{\theta_m} L_s)$ gradients. It then updates ML function $\phi(y_m^t; \theta_m)$ and communicates states $-(x_m^t)_c, (x_m^t)_a$ to the server.
2. **Server.** The server processes $(x_m^t)_c, (x_m^t)_a$ from all M clients with a *global non-linear ML* $f_s(\cdot)$ to *globally encode interdependencies*. The server minimizes its loss L_s and updates its global ML function f_s . It then communicates gradients $\nabla_{(x_m^t)_a} L_s$ to the respective clients.

The motivation behind the problem (interdependencies in OT clients), and the methodology of learning interdependencies in a federated setting is depicted in Fig. 1.

The trained framework captures the cross-client interdependencies as *non-interpretable parameters* of ML functions (i.e., ϕ_m, f_s). Thus, the framework can detect any local anomalies but lacks root cause analysis capabilities. To address this, we perform the following during inference:

1. **Client.** Detect anomalies locally using residual analysis-based binary anomaly flags Z_c and Z_a from the proprietary and augmented client models, respectively. Each client communicates their anomaly flag pair (Z_c, Z_a) to the server.
2. **Server.** The server then leverages the framework’s understanding of cross-client interdependencies to distinguish between the clients that are associated with *root cause* of an anomaly and those experiencing its *propagated effect*.

4 Training: Learning Cross-Client Interdependencies

4.1 Proprietary Client Model

Model. To handle non-linear dynamics, the proprietary client models are assumed to be *Extended Kalman Filters* (EKF). Each client m utilizes local data $y_m \in \mathbb{R}^{D_m}$ to compute states as follows:

$$(x_m^t)_c = f_m((\hat{x}_m^{t-1})_c), \quad \text{and} \quad (\hat{x}_m^t)_c = (x_m^t)_c + K_m^c(y_m^t - h_m((x_m^t)_c)) \quad (1)$$

where $(\hat{x}_m^t)_c \in \mathbb{R}^{P_m}$, and $(x_m^t)_c \in \mathbb{R}^{P_m}$ are the estimated and predicted states. $f_m(\cdot)$ defines local state transitions, and $h_m(\cdot)$ maps states to observations, and K_m^c is the Kalman gain computed as:

$$K_m^c = P_m^- H_m^\top (H_m P_m^- H_m^\top + R_m)^{-1}, \quad \text{with} \quad P_m^- = F_m P_m F_m^\top + Q_m \quad (2)$$

where, $H_m = \frac{\partial h_m}{\partial x} \Big|_{(x_m^t)_c}$, and P_m^- and R_m represent the covariance of predicted state and measurement noise, respectively. Similarly, $F_m = \frac{\partial f_m}{\partial x} \Big|_{(\hat{x}_m^{t-1})_c}$, P_m and Q_m are the covariance of the estimated state and process noise respectively.

Limitation. The local state transition function $f_m(\cdot)$ models only client m 's dynamics using local data y_m^t and state $(\hat{x}_m^{t-1})_c$. Thus, it **fails to capture cross-client interdependencies** due to the lack of access to information (raw data or states) from other clients (i.e., \forall clients $i \in M \setminus \{m\}$).

4.2 Augmented Client Model

State Augmentation. To address this limitation, the proprietary client model is *augmented* with a *non-linear ML* function $\phi_m(y_m^t; \theta_m)$, parameterized by θ_m , as follows:

$$(\hat{x}_m^t)_a = (\hat{x}_m^t)_c + \phi_m(y_m^t; \theta_m), \quad \text{and} \quad (x_m^t)_a = f_m((\hat{x}_m^{t-1})_a) \quad (3)$$

Loss Function and Param. Update. The augmented client model minimizes a *reconstruction loss* $(L_m)_a$ defined as: $(L_m)_a = \|y_m^t - h_m((x_m^t)_a)\|_2^2$. The client parameters θ_m are then updated as:

$$\theta_m^{k+1} = \theta_m^k - \eta_1 \nabla_{\theta_m^k} (L_m)_a - \eta_2 \nabla_{\theta_m^k} (L_s), \quad \text{with} \quad \nabla_{\theta_m^k} (L_s) = (\nabla_{(x_m^t)_a} (L_s)) \cdot (\nabla_{\theta_m^k} (x_m^t)_a) \quad (4)$$

where $\nabla_{(x_m^t)_a} (L_s)$ is communicated from the server, and $\nabla_{\theta_m^k} (x_m^t)_a$ is computed locally.

Client to Server. Each client m communicates the tuple of states $[(\hat{x}_m^{t-1})_c, (x_m^t)_a]$ to the server.

4.3 Global Server Model

The server model uses a *non-linear ML* f_s , serving as a proxy for a global state transition function. It predicts the future state of all M clients using the current state estimates (received from the clients):

$$\{(x_m^t)_s\}_{m=1}^M = f_s(\{(\hat{x}_m^{t-1})_c\}_{m=1}^M; \theta_s). \quad (5)$$

Loss Function and Param. Update. The server minimizes the *mean squared error* between its predicted and client's augmented states: $(L_s) = \sum_{m=1}^M \|(x_m^t)_s - (x_m^t)_a\|_2^2$. It then updates θ_s as:

$$\theta_s^{k+1} = \theta_s^k - \eta_3 \nabla_{\theta_s^k} (L_s) \quad (6)$$

Server to Client: The server communicates the gradient $\nabla_{(x_m^t)_a} (L_s)$ to each client m , enabling update of client model's parameter θ_m . Algorithm 1 (see Appendix) provides the steps for training.

5 Inference: Root Cause Analysis

During inference **the server aims to identify the root cause of an anomaly without access to client states or raw data (decentralized)**. This is different from a complete causal discovery, which requires extensive conditional independence tests. Prior works [23, 27, 44, 53] similarly focus on root cause identification but in centralized settings.

Metric. An anomaly can be detected when a vector r has a significant deviation from its nominal behavior. If μ and Σ represent the mean and covariance of r then we quantify this deviation as $d_M^2(\cdot)$,

Table 1: RCA for any two pair of clients C_1 and C_2 at any time t using the anomaly flags

Client C_1 (Z_c, Z_a)	Client C_2 (Z_c, Z_a)	RCA (RC, PE)	Client C_1 (Z_c, Z_a)	Client C_2 (Z_c, Z_a)	RCA (RC, PE)
(1, 1)	(0, 0)	($C_1, -$)	(1, 0)	(1, 1)	(C_2, C_1)
(0, 0)	(1, 1)	($C_2, -$)	(0, 0)	(0, 0)	No anomaly
(1, 1)	(1, 0)	(C_1, C_2)	(1, 0)	(1, 0)	(Neither, Both)
(0, 1)	(1, 1)	Imperfect training	(0, 1)	(0, 1)	Independent Clients
(1, 1)	(0, 1)	Imperfect training	(1, 1)	(1, 1)	Violates Assumptions

which is further used to generate a binary anomaly flag Z as given in eq 7. The threshold τ is derived statistically from the vector r , **only during nominal operation** of the client.

$$d_M^2(r) = (r - \mu)^\top \Sigma^{-1} (r - \mu), \quad \text{and} \quad Z = \begin{cases} 1, & \text{if } d_M^2(r) > \tau \text{ (anomaly)}, \\ 0, & \text{otherwise} \end{cases} \quad (7)$$

Anomaly Detection. Each client m is equipped with two models **(1)** a proprietary client model, and **(2)** an augmented client model, generating residuals $(r_m^t)_c$, and $(r_m^t)_a$, respectively:

$$(r_m^t)_c = y_m^t - h_m((x_m^t)_c), \quad \text{and} \quad (r_m^t)_a = y_m^t - h_m((x_m^t)_a) \quad (8)$$

These residuals are an integral part of the client models, appearing in eq 1 and the *loss function* of the augmented client model, respectively. They can be interpreted as the error in reconstructing the raw data y_m^t using the two client models. For the remainder of this section, we drop indices m and t for notational brevity. Using r_c and r_a , the client models can generate anomaly flags Z_c , and Z_a respectively. With τ_c and τ_a as thresholds for the proprietary and augmented models respectively,

$$Z_c = \begin{cases} 1, & \text{if } d_M^2(r_c) > \tau_c, \\ 0, & \text{otherwise.} \end{cases}, \quad \text{and} \quad Z_a = \begin{cases} 1, & \text{if } d_M^2(r_a) > \tau_a \\ 0, & \text{otherwise.} \end{cases} \quad (9)$$

Communication (Inference). Clients communicate the anomaly flags Z_c and Z_a to the server.

Root Cause Analysis. For any client, when $Z_a = 1$, the client detects an anomaly. Since the augmented model is expected to learn interdependencies, so $Z_a = 1$ confirms a local fault (given interdependent clients and perfect training), **not** caused by interdependencies. Conversely, $Z_c = 1$ indicates an anomaly that **might be** interdependency-driven (propagation of effects).

Given the above logic, we can say that the anomaly associated with a *root cause* (RC) client originates from a local fault within that client, and identified when $(Z_c, Z_a) = (1, 1)$. On the contrary, a *propagated effect* (PE) occurs due to interdependency with the RC client, identified when $(Z_c, Z_a) = (1, 0)$. For any two clients C_1 , and C_2 , Table 1 provides a look-up table for RCA.

Remark 5.1. A flag $(Z_c, Z_a) = (1, 1)$ from an isolated client at a single time instant **cannot** confirm it as the RC, as it may be a false alarm, likely due to *imperfect training* of the framework. PEs offer critical contextual evidence by revealing anomaly spread among interdependent clients. RCA requires monitoring (Z_c, Z_a) across all clients over a long time horizon to identify consistent patterns.

Assumptions. The federated RCA methodology makes the following assumptions:

- **No Feedback Loops.** The underlying causal structure of the system is a directed acyclic graph.
- **Causal Sufficiency.** All clients share their anomaly flags and there are no latent confounders.
- **Multiple RCs.** RC anomalies occurring at any client follow a Poisson arrival process.

Proposition 5.2. For M clients, let $N_m(\Delta t)$ represent the number of root cause anomalies occurring at C_m within time Δt . The probability of multiple clients experiencing root causes in Δt is negligible for small Δt , i.e., $P\left(\sum_{m=1}^M N_m(\Delta t) > 1\right) \rightarrow 0$ as $\Delta t \rightarrow 0$.

Proposition 5.2 ensures that multiple clients **cannot** share root causes anomalies simultaneously. Thus, there is always a unique root cause client that can be identified using Table 1. The pseudocode for inference is provided in Algorithm 2 of the Appendix.

6 Convergence Analysis

This section demonstrated that the proposed framework’s performance converges to a centralized oracle, confirming the framework’s understanding of interdependencies.

Definition 6.1 (Centralized Oracle). An *Extended Kalman Filter* that utilizes data from all M clients, represented as y^t , to predict the one-step ahead state x_o^t and estimate the current state \hat{x}_o^t :

$$x_o^t = f(\hat{x}_o^{t-1}) \quad \text{and} \quad \hat{x}_o^t = x_o^t + K^o(y_o^t - h(x_o^t)) \quad (10)$$

where K^o is defined similar to the proprietary client model's K_m^c , with the difference that the Jacobians in the oracle are $F = \frac{\partial f}{\partial x}|_{\hat{x}_o^{t-1}}$, and $H = \frac{\partial h}{\partial x}|_{\hat{x}_o^{t-1}}$. We utilize an operator $Extract_m$ to isolate the components of a vector (e.g., $x_o^t, \hat{x}_o^t, y_o^t$) or the sub-matrix of a matrix (e.g., K^o) corresponding only to client m .

Assumption 6.2. The client loss function $(L_m)_a$ is convex and \mathcal{L}_{L_m} -Lipschitz smooth w.r.t. θ_m .

Assumption 6.3. The non-linear local ML function $\phi_m(y_m^t; \theta_m)$ is \mathcal{L}_{θ_m} -Lipschitz w.r.t. θ_m .

Definition 6.4 (Irreducible Local Error ϵ^*). Consider the optimal parameter θ_m^* for the local ML function $\phi_m(\cdot; \theta)$. The *irreducible local error* $\epsilon^* := \mathbb{E}[\|\phi_m(y_m^{t-1}; \theta_m^*) - \sum_{n \neq m} (\hat{x}_n^{t-1})_o\|]$ is the discrepancy between the optimal local ML prediction and the sum of other clients' states.

If trained perfectly, ϵ^* may be negligible or zero; otherwise, it quantifies the **training error of the local ML model in capturing interdependencies** across clients.

Lemma 6.5 (Local Learning of Interdependency). For fixed step size $\eta_1, \eta_2 \leq 1/L$, we obtain, $\mathbb{E}[\|\phi_m(y_m^{t-1}; \theta_m^k) - \sum_{n \neq m} (\hat{x}_n^{t-1})_o\|] \leq \mathcal{L}_{\theta_m} \|\theta_m^k - \theta_m^*\| + \epsilon^*$. As $k \rightarrow \infty$, $\|\theta_m^k - \theta_m^*\| \rightarrow 0$, and the limit of the above norm difference is bounded by ϵ^* .

Lemma 6.5 shows that the **local ML function at each client approximates the contribution from other clients**. Next we assume bounds on the terms involved in the EKF-based proprietary client model to prove the convergence of our decentralized framework to the centralized oracle.

Assumption 6.6. The states of each client m is bounded, i.e., $\mathbb{E}[\|(x_m^t)_o\|] \leq C_x \forall t$, where $C_x > 0$.

Assumption 6.7. The (local) state transition function $f_m(\cdot)$ and the measurement function $h_m(\cdot)$ are Lipschitz continuous with Lipschitz constants \mathcal{L}_{f_m} and \mathcal{L}_{h_m} , respectively.

The state transition functions of the proprietary client model and the centralized oracle **differ structurally**. Each client m uses f_m in its local client model, while the centralized oracle uses f and performs $Extract_m(f(\mathbf{z}))$. Proposition 6.8 shows that the structural difference is bounded.

Proposition 6.8 (Structural Diff.). For client m , $\exists \delta_m$ s.t., $\mathbb{E}[\|f_m(z_m) - Extract_m(f(\mathbf{z}))\|] \leq \delta_m$.

Definition 6.9 (Residual of Centralized Oracle). For any client m , the residual of the EKF-based centralized oracle is given by $(r_m^t)_o := y_m^t - h_m((x_m^t)_o)$.

Theorem 6.10 (Local Convergence to Oracle). Let $\Delta K_m := K_m^c - Extract_m(K^o)$. Then, for fixed step sizes $\eta_1, \eta_2 \leq 1/L$, if $1 + \|\Delta K_m\| \mathcal{L}_{h_m} < \frac{1}{\mathcal{L}_{f_m}}$ then the predicted state of the augmented client model $(x_m^{t,k})_a$ converges to that of a centralized oracle $(x_m^t)_o$ in steady state: $\lim_{k \rightarrow \infty} \mathbb{E}[\|(x_m^{t,k})_a - (x_m^t)_o\|] = \mathcal{O}(\mathcal{L}_{f_m}(\rho + \epsilon^*) + \delta_m)$ where, $\rho := \frac{\|\Delta K_m\| \sup_t \|(r_m^t)_o\| + \mathcal{L}_{h_m} C_x + \mathcal{L}_{f_m} (M-1) C_x}{1 - (1 + \|\Delta K_m\| \mathcal{L}_{h_m}) \mathcal{L}_{f_m}}$.

Theorem 6.10 shows that the predicted state of the augmented client model converges to that of a centralized oracle in the steady state. For **perfect learning of interdependency** ($\epsilon^* \rightarrow 0$) and **small structural difference** ($\delta_m \rightarrow 0$), the augmented client model converges to the centralized oracle up to a constant $\mathcal{L}_{f_m} \rho$. This constant is a function of the parameters of the state space models.

Definition 6.11 (Irreducible Global Error). The *irreducible global error* σ^* is defined as $\sigma^* := \mathbb{E}[\|f_s(\{(\hat{x}_m^t)_c\}_{m=1}^M; \theta_s^*) - f(\hat{x}_o^t)\|]$ where θ_s^* represents the optimal param. of the server model.

This error captures the **training error of the global ML model in capturing interdependencies** across all M clients. When trained perfectly, the server converges to the centralized oracle or, $\sigma^* \rightarrow 0$.

Assumption 6.12. f_s of the global server model is \mathcal{L}_{f_s} -Lipschitz continuous w.r.t to its input.

Theorem 6.13 (Global Server Convergence to Oracle). Let $\Delta K_m := K_m^c - Extract_m(K^o)$. Then, for fixed learning rates $\eta_3 \leq 1/L$, if $1 + \|\Delta K_m\| \mathcal{L}_{h_m} < \frac{1}{\mathcal{L}_{f_m}}$, the predicted state of the global server model $(x_s^{t,k})$ converges to that of a centralized oracle (x_o^t) in steady state: $\lim_{k \rightarrow \infty} \mathbb{E}[\|x_s^{t,k} - x_o^t\|] = \mathcal{O}(\mathcal{L}_{f_s} M \rho + \sigma^*)$ where, $\rho := \frac{\|\Delta K_m\| \sup_t \|(r_m^t)_o\| + \mathcal{L}_{h_m} C_x + \mathcal{L}_{f_m} (M-1) C_x}{1 - (1 + \|\Delta K_m\| \mathcal{L}_{h_m}) \mathcal{L}_{f_m}}$.

The result presented in Theorem 6.13 implies that the **understanding of interdependencies by the server model converges to that of a centralized oracle** up to a constant depending on the parameters of the state space models, and the irreducible error of the global server model.

7 Privacy Analysis

In this section we analyze how communications during training and inference are protected to prevent revealing sensitive client data. During training, the communicated local and augmented client models' states can be perturbed as $(\tilde{x}_m^{t-1})_c = (\hat{x}_m^{t-1})_c + \mathcal{N}(0, \sigma_c^2)$ and $(\tilde{x}_m^t)_a = (x_m^t)_a + \mathcal{N}(0, \sigma_a^2)$.

Theorem 7.1 (Client-to-Server Communication). *At each time step t , the mechanisms by which client m sends $(\tilde{x}_m^{t-1})_c$ (state communication) and $(\tilde{x}_m^t)_a$ (augmented communication) to the server satisfy (ϵ, δ) -differential privacy w.r.t. the client's local data y_m^t . This is achieved by adding Gaussian noise with standard deviations: $\sigma_c \geq \frac{2\|\Delta K_m\|(\mathcal{L}_{h_m} C_x + \sup_t \|r_m^t\|)\sqrt{2\ln(1.25/\delta_c)}}{\epsilon_c}$, $\sigma_a \geq \frac{2(\mathcal{L}_{f_m} C_x + \mathcal{L}_{\theta_m} \sup_t \|y_m^t\|)\sqrt{2\ln(1.25/\delta_a)}}{\epsilon_a}$. The total privacy budget is $\epsilon = \epsilon_c + \epsilon_a$ and $\delta = \delta_c + \delta_a$.*

Theorem 7.1 says that the proprietary and augmented client states sent to the server can be perturbed with noise proportional to their sensitivities, preventing leakage of client data. When the server communicates back to the clients, the gradients $g_m^t := (\nabla_{(\hat{x}_m^t)_a} L_s)$ can be perturbed as: $\tilde{g}_m^t = \text{clip}(g_m^t, C_g) + \mathcal{N}(0, \sigma_g^2)$, where $\text{clip}(g_m^t, C_g)$ scales $\|g_m^t\|_2$ to C_g if $\|g_m^t\|_2 > C_g$.

Theorem 7.2 (Server-to-Client Communication). *At each time step t , the mechanism by which the server sends \tilde{g}_m^t (gradient updates) to client m satisfies (ϵ, δ) -differential privacy w.r.t. any single client's data. The sensitivity of the clipped gradient is bounded by $C_g := \max_t \|g_m^t\|_2$, and Gaussian noise with standard deviation: $\sigma_g \geq \frac{2C_g\sqrt{2\ln(1.25/\delta)}}{\epsilon}$, is added to ensure privacy.*

Theorem 7.2 guarantees that gradients sent by the server can be perturbed, protecting data of any single client. Similar to training, during inference, the binary anomaly flags can be perturbed with Bernoulli noise, resulting in Theorem 7.3.

Theorem 7.3 (Privacy during Inferencing). *During inference, the mechanism by which each client communicates \tilde{Z}_c^t and \tilde{Z}_a^t satisfies ϵ -differential privacy w.r.t. the client's residuals. This is achieved through randomized response with probabilities $p_c = \frac{e^{\epsilon_c}}{1+e^{\epsilon_c}}$ and $p_a = \frac{e^{\epsilon_a}}{1+e^{\epsilon_a}}$.*

8 Experiments

8.1 Synthetic Datasets

Data Generation. We simulate an M -client non-linear state-space model where the root cause client evolves as: $x_m^t = f_m(x_m^{t-1}) + \epsilon_m$, and clients exhibiting propagated effects follow: $x_n^t = f_n(x_n^{t-1}) + g_{dep}^n(x_m^{t-1}) + \epsilon_n$, with $\epsilon_m \sim \mathcal{N}(0, Q_m) \forall m$. Directed interdependencies are captured in $g_{dep}^n(x_m^{t-1})$. Raw data are mapped via $y_m^t = h_m(x_m^t) + \zeta_m$, where $\zeta_m \sim \mathcal{N}(0, R_m) \forall m$. For all M clients, $f_m(\cdot)$ and $g_{dep}^m(\cdot)$ are modeled as LSTMs, while $h_m(\cdot)$ are implemented as fully connected networks. The “**Architectural details**” of f_m, h_m, g_{dep} are in the Appendix. Except for “**Scalability studies**”, experiments use $M = 2, D_m = 4$, and $P_m = 2 \forall m \in \{1, 2\}$ to ensure a controlled and interpretable evaluation. The true network structure follows $C_1 \rightarrow C_2$, with C_1 influencing C_2 . Due to space limitations, further details on “**Experimental Settings**” are provided in the Appendix.

Learning Interdependencies. After training, we assess the framework's ability to learn cross-client interdependencies. Fig. 2 shows state correlations in synthetic datasets, where augmented client models and the server model closely match the centralized oracle, differing significantly from proprietary client models. This highlights their effectiveness in capturing cross-client interdependencies.

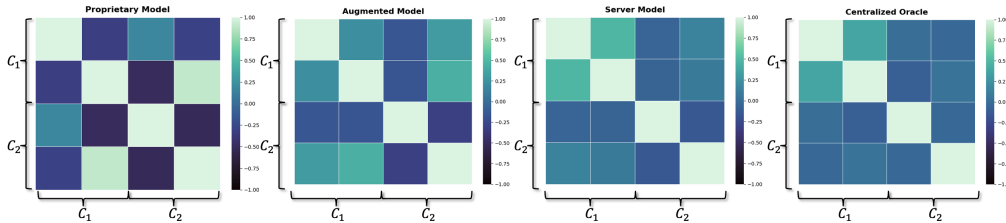


Figure 2: Correlation in the states of clients C_1 , and C_2 in their proprietary model (left), augmented model (second to the left), server model (second to the right), and centralized oracle (right)

Baselines. We compare against the following baselines: (1) *Only Proprietary Model*: EKF-based proprietary client models without local ML augmentation or a global server model, evaluating the limitations relying solely on local data. (2) *Without Proprietary Model*: Clients use end-to-end ML instead of EKF-based proprietary models, testing the performance without a domain-specific proprietary model. (3) *Pre-trained Clients [33]*: Clients pre-train augmented models independently and share state representations for training a global server model, assessing the impact of federated interdependency learning without continuous server feedback. (4) *Centralized Oracle*: An EKF with access to all client states and raw data, serving as an upper bound with known interdependencies.

Evaluation Metric. Anomaly detection is evaluated using (1) ARL_0 , which measures the expected time passed before a false alarm under nominal conditions, and (2) ARL_1 , which quantifies the average time to detect a true anomaly. RCA performance is assessed with (1) *Precision*, the proportion of correctly identified RCs, and (2) *Recall*, the proportion of true RCs successfully identified.

Anomaly Detection. The inference step for all four baselines follows the procedure in Section 5, utilizing anomaly flags for RCA. Thresholds τ_c and τ_a are computed statistically using nominal data. The anomaly detection for synthetic datasets is given in Table 2. The *Only Proprietary Model*, which does not use ML or encode any interdependencies, achieves the highest ARL_0 (fewest false alarms) but suffers from the highest ARL_1 (slowest detection). Despite being decentralized, our approach achieves the close enough performance as the *Centralized Oracle*, which has direct access to interdependencies g_{dep} . Furthermore, our approach provides same ARL values as *Pre-trained Clients* and *Without Proprietary Model* baselines, suggesting the dominance of ML in detection.

Table 2: Performance of anomaly detection and root cause analysis approach discussed in Section 5

Model Used	Anomaly Detection		Root Cause Analysis (RCA)		
	ARL_0	ARL_1	Precision	Recall	F_1 score
Only Proprietary Model	36.88	157.8	Cannot perform RCA as Z_a is absent		
Without Proprietary Model	27.82	112.38	Cannot perform RCA as Z_c is absent		
Pre-trained Clients	27.82	112.38	0.70	0.49	0.576
Our Framework	27.82	112.38	0.73	0.57	0.640
Centralized Oracle	22.9	112.75	Trivial with known interdependencies		

Root Cause Analysis. Once the anomalies are detected, we perform RCA on the entire system. Table 2 provides the performance for our approach and *Pre-trained Clients*. Since *Only Proprietary Client Model*, and *Without Proprietary Client Model* **do not have Z_a , and Z_c respectively**, we **cannot utilize our RCA approach for them**. Furthermore, *Centralized Oracle* has access to interdependencies, making it trivial for RCA. Our approach achieves high precision, without direct access to interdependencies. However, its low recall suggests potential gaps in identifying all root causes, warranting further refinement in our federated RCA approach. Despite same anomaly detection performance, our method marginally outperforms *Pre-trained Clients*, emphasizing the advantages of server-to-client communication in RCA.

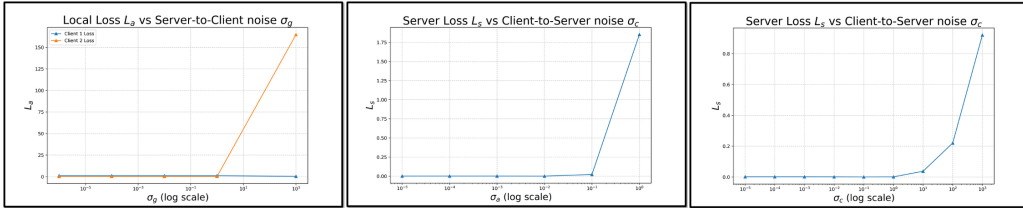


Figure 3: Loss under Gaussian noise in (a) server-to-client and (b-c) client-to-server communications.

Privacy Analysis. We add Gaussian noise with varying standard deviation to communications: (i) server-to-client and (ii) client-to-server (Fig. 3). We observe that server and client losses remain stable until impractically high noise levels (10^4 and 10^5 respectively), demonstrating training robustness under privacy constraints. We also investigate performance evaluation of (i) anomaly detection and (ii) root cause analysis (Fig. 4) under randomized anomaly flags. Metrics remain stable with varying p_c (i.e., noise added to Z_c) but show sensitivity to changes in p_a (i.e., noise in Z_a).

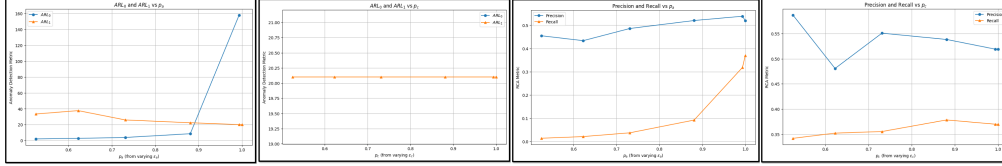


Figure 4: Anomaly detection performance showing (a) sensitivity to p_a and (b) robustness to p_c . RCA performance under randomized anomaly flags showing sensitivity to (c) p_a and (d) p_c

Scalability Studies. We assess the framework’s scalability by analyzing the final training loss as a function of communication cost per round. We vary the number of clients ($M \in \{2, 4, 8, 16\}$) keeping the state and data dimensions fixed. Table 3 gives the server loss (L_s) vs. comm. overhead.

Table 3: Scalability Studies

Comm. Overhead (bytes/round)	Server Loss (L_s)	Comm. Overhead (bytes/round)	Server Loss (L_s)
32	0.0305	128	0.0263
64	0.0129	256	0.0412

Threshold Sensitivity. All previous experiments were conducted with τ_a set at the 95th percentile of Mahalanobis distance. The framework’s sensitivity to different τ_a is studied in the Appendix.

8.2 Real-world Industrial Dataset

Description. We evaluate our framework on a real-world industrial cybersecurity dataset: *Hardware-In-the-Loop Augmented Industrial Control System (HAI)* [45]. HAI emulates steam-turbine and pumped-storage hydropower generation, comprising four processes— *Boiler*, *Turbine*, *Water Treatment*, and *HIL Simulation*, each treated as a separate client. The dataset includes cyberattacks that introduce anomalies in a single process (client), which propagate due to inter-process dependencies.

We specify the “*Experimental Settings*”, and “*Pre-processing Steps*” in the Appendix.

Training. We train the dataset on the testbed’s nominal operation (i.e., no cyberattacks) to learn cross-client interdependencies. Results (provided in the Appendix) depict that the framework learned a correlation between the *Boiler*, *Turbine*, *Water Treatment* processes without moving the sensor data.

Inference. The test dataset includes cyberattack-based anomalies in the testbed’s operation. The ground-truth label of the anomaly, as well as documentation on the root cause, are also provided for validation. We use our methodology to detect these anomalies and identify the root cause process. Due to space limitations, we provide the results in the Appendix.

9 Conclusion and Limitations

This work proposes a federated cross-client interdependency learning framework that enables RCA in decentralized industrial systems with nonlinear and heterogeneous IoT data. The approach augments unmodifiable proprietary client models with local ML components and coordinates interdependency learning through a central server. Anomalies are detected locally, and only binary flags are shared with the server for a decentralized RCA. The method is evaluated on synthetic and real-world industrial dataset, validating the claims made about interdependency learning and RCA.

Our method has certain key limitations: RCA is performed only at the server, requiring clients to share anomaly flags to confirm root causes. The convergence analysis assumes proprietary client models follow an EKF structure, limiting generalizability to other model types. Empirical performance is sensitive to threshold, data noise, and the architecture of EKF, ML, and interdependency functions.

References

- [1] Charles K Assaad, Imad Ez-Zejjari, and Lei Zan. Root cause identification for collective anomalies in time series given an acyclic summary causal graph with loops. In *International Conference on Artificial Intelligence and Statistics*, pages 8395–8404. PMLR, 2023.
- [2] Kailash Budhathoki, Lenon Minorics, Patrick Bloebaum, and Dominik Janzing. Causal structure-based root cause analysis of outliers. In *Proceedings of the 39th International Conference on Machine Learning*, pages 2357–2369. PMLR, June 2022.
- [3] Sergey V Buldyrev, Roni Parshani, Gerald Paul, H Eugene Stanley, and Shlomo Havlin. Catastrophic cascade of failures in interdependent networks. *Nature*, 464(7291):1025–1028, 2010.
- [4] Ye Cai, Yijia Cao, Yong Li, Tao Huang, and Bin Zhou. Cascading Failure Analysis Considering Interaction Between Power Grids and Communication Networks. *IEEE Transactions on Smart Grid*, 7(1):530–538, January 2016.
- [5] Timothy Castiglia, Yi Zhou, Shiqiang Wang, Swanand Kadhe, Nathalie Baracaldo, and Stacy Patterson. Less-vfl: Communication-efficient feature selection for vertical federated learning. In *Proceedings of the 40th International Conference on Machine Learning*, page 3757–3781. PMLR, July 2023.
- [6] Timothy J. Castiglia, Anirban Das, Shiqiang Wang, and Stacy Patterson. Compressed-vfl: Communication-efficient learning with vertically partitioned data. In *Proceedings of the 39th International Conference on Machine Learning*, page 2738–2766. PMLR, June 2022.
- [7] Fahao Chen, Peng Li, Toshiaki Miyazaki, and Celimuge Wu. Fedgraph: Federated graph learning with intelligent sampling. *IEEE Transactions on Parallel and Distributed Systems*, 33(8):1775–1786, 2021.
- [8] Jiayi Chen and Aidong Zhang. Fedmsplit: Correlation-adaptive federated multi-task learning across multimodal split networks. In *Proceedings of the 28th ACM SIGKDD Conference on Knowledge Discovery and Data Mining, KDD '22*, page 87–96, New York, NY, USA, August 2022. Association for Computing Machinery.
- [9] Pengfei Chen, Yong Qi, and Di Hou. Causeinfer: Automated end-to-end performance diagnosis with hierarchical causality graph in cloud environment. *IEEE Transactions on Services Computing*, 12(2):214–230, 2019.
- [10] Tianyi Chen, Xiao Jin, Yuejiao Sun, and Wotao Yin. Vaf1: a method of vertical asynchronous federated learning. (arXiv:2007.06081), Jul 2020. number: arXiv:2007.06081 arXiv:2007.06081 [cs, math, stat].
- [11] Kewei Cheng, Tao Fan, Yilun Jin, Yang Liu, Tianjian Chen, Dimitrios Papadopoulos, and Qiang Yang. Secureboost: A lossless federated learning framework. *IEEE Intelligent Systems*, 36(6):87–98, November 2021.
- [12] Lei Cui, Youyang Qu, Gang Xie, Deze Zeng, Ruidong Li, Shigen Shen, and Shui Yu. Security and privacy-enhanced federated learning for anomaly detection in iot infrastructures. *IEEE Transactions on Industrial Informatics*, 18(5):3492–3500, May 2022.
- [13] Bamdad Falahati, Yong Fu, and Lei Wu. Reliability Assessment of Smart Grid Considering Direct Cyber-Power Interdependencies. *IEEE Transactions on Smart Grid*, 3(3):1515–1524, September 2012.
- [14] Jiamin Fan, Guoming Tang, Kui Wu, Zhengan Zhao, Yang Zhou, and Shengqiang Huang. Score-vae: Root cause analysis for federated-learning-based iot anomaly detection. *IEEE Internet of Things Journal*, 11(1):1041–1053, 2023.
- [15] Astha Garg, Wenyu Zhang, Jules Samaran, Ramasamy Savitha, and Chuan-Sheng Foo. An evaluation of anomaly detection and diagnosis in multivariate time series. *IEEE Transactions on Neural Networks and Learning Systems*, 33(6):2508–2517, June 2022.

- [16] Philipp Geiger, Kun Zhang, Bernhard Schölkopf, Mingming Gong, and Dominik Janzing. Causal inference by identification of vector autoregressive processes with hidden components. In Francis Bach and David Blei, editors, *Proceedings of the 32nd International Conference on Machine Learning*, volume 37 of *Proceedings of Machine Learning Research*, pages 1917–1925, Lille, France, 07–09 Jul 2015. PMLR.
- [17] Clive WJ Granger. Testing for causality: A personal viewpoint. *Journal of Economic Dynamics and Control*, 2:329–352, 1980.
- [18] Bin Gu, An Xu, Zhouyuan Huo, Cheng Deng, and Heng Huang. Privacy-preserving asynchronous vertical federated learning algorithms for multiparty collaborative learning. *IEEE Transactions on Neural Networks and Learning Systems*, page 1–13, 2021.
- [19] Chaoyang He, Keshav Balasubramanian, Emir Ceyani, Carl Yang, Han Xie, Lichao Sun, Lifang He, Liangwei Yang, Philip S Yu, Yu Rong, et al. Fedgraphnn: A federated learning system and benchmark for graph neural networks. *arXiv preprint arXiv:2104.07145*, 2021.
- [20] Yaochen Hu, Di Niu, Jianming Yang, and Shengping Zhou. Fdml: A collaborative machine learning framework for distributed features. In *Proceedings of the 25th ACM SIGKDD International Conference on Knowledge Discovery & Data Mining*, KDD '19, page 2232–2240, New York, NY, USA, Jul 2019. Association for Computing Machinery.
- [21] Lingxiao Huang, Zhize Li, Jialin Sun, and Haoyu Zhao. Coresets for vertical federated learning: Regularized linear regression and k -means clustering. *Advances in Neural Information Processing Systems*, 35:29566–29581, December 2022.
- [22] Truong Thu Huong, Ta Phuong Bac, Dao Minh Long, Tran Duc Luong, Nguyen Minh Dan, Le Anh Quang, Le Thanh Cong, Bui Doan Thang, and Kim Phuc Tran. Detecting cyberattacks using anomaly detection in industrial control systems: A federated learning approach. *Computers in Industry*, 132:103509, November 2021.
- [23] Azam Ikram, Sarthak Chakraborty, Subrata Mitra, Shiv Saini, Saurabh Bagchi, and Murat Kocaoglu. Root cause analysis of failures in microservices through causal discovery. In S. Koyejo, S. Mohamed, A. Agarwal, D. Belgrave, K. Cho, and A. Oh, editors, *Advances in Neural Information Processing Systems*, volume 35, pages 31158–31170. Curran Associates, Inc., 2022.
- [24] Rex B Kline. *Principles and practice of structural equation modeling*. Guilford publications, 2023.
- [25] Mingjie Li, Zeyan Li, Kanglin Yin, Xiaohui Nie, Wenchi Zhang, Kaixin Sui, and Dan Pei. Causal Inference-Based Root Cause Analysis for Online Service Systems with Intervention Recognition. In *Proceedings of the 28th ACM SIGKDD Conference on Knowledge Discovery and Data Mining*, KDD '22, pages 3230–3240, New York, NY, USA, August 2022. Association for Computing Machinery.
- [26] Songze Li, Duanyi Yao, and Jin Liu. Fedvs: Straggler-resilient and privacy-preserving vertical federated learning for split models. In *Proceedings of the 40th International Conference on Machine Learning*, page 20296–20311. PMLR, July 2023.
- [27] Cheng-Ming Lin, Ching Chang, Wei-Yao Wang, Kuang-Da Wang, and Wen-Chih Peng. Root cause analysis in microservice using neural granger causal discovery. In *Proceedings of the AAAI Conference on Artificial Intelligence*, volume 38, pages 206–213, 2024.
- [28] Chao Liu, Kin Gwn Lore, Zhanhong Jiang, and Soumik Sarkar. Root-cause analysis for time-series anomalies via spatiotemporal graphical modeling in distributed complex systems. *Knowledge-Based Systems*, 211:106527, January 2021.
- [29] Chao Liu, Kin Gwn Lore, and Soumik Sarkar. Data-driven root-cause analysis for distributed system anomalies. In *2017 IEEE 56th Annual Conference on Decision and Control (CDC)*, pages 5745–5750, December 2017.

- [30] Yi Liu, Sahil Garg, Jiangtian Nie, Yang Zhang, Zehui Xiong, Jiawen Kang, and M. Shamim Hosain. Deep anomaly detection for time-series data in industrial iot: A communication-efficient on-device federated learning approach. *IEEE Internet of Things Journal*, 8(8):6348–6358, April 2021.
- [31] Yijing Liu, Dongming Han, Jianwei Zhang, Haiyang Zhu, Mingliang Xu, and Wei Chen. Federated multi-task graph learning. *ACM Transactions on Intelligent Systems and Technology*, 13(5):80:1–80:27, June 2022.
- [32] Helmut Lütkepohl. *New Introduction to Multiple Time Series Analysis*. Springer, 2005.
- [33] Tengfei Ma, Trong Nghia Hoang, and Jie Chen. Federated learning of models pre-trained on different features with consensus graphs. In *Proceedings of the Thirty-Ninth Conference on Uncertainty in Artificial Intelligence*, UAI '23. JMLR.org, 2023.
- [34] Peihua Mai and Yan Pang. Vertical federated graph neural network for recommender system. In *International Conference on Machine Learning*, pages 23516–23535. PMLR, 2023.
- [35] Othmane Marfoq, Giovanni Neglia, Aurélien Bellet, Laetitia Kameni, and Richard Vidal. Federated multi-task learning under a mixture of distributions. In *Advances in Neural Information Processing Systems*, volume 34, page 15434–15447. Curran Associates, Inc., 2021.
- [36] Brendan McMahan, Eider Moore, Daniel Ramage, Seth Hampson, et al. Communication-efficient learning of deep networks from decentralized data. *Proceedings of the 20th International Conference on Artificial Intelligence and Statistics*, 2017.
- [37] Igor Melnyk and Arindam Banerjee. Estimating structured vector autoregressive models. In Maria Florina Balcan and Kilian Q. Weinberger, editors, *Proceedings of The 33rd International Conference on Machine Learning*, volume 48 of *Proceedings of Machine Learning Research*, pages 830–839, New York, New York, USA, 20–22 Jun 2016. PMLR.
- [38] Chuizheng Meng, Sirisha Rambhatla, and Yan Liu. Cross-node federated graph neural network for spatio-temporal data modeling. In *Proceedings of the 27th ACM SIGKDD conference on knowledge discovery & data mining*, pages 1202–1211, 2021.
- [39] Osman Mian, David Kaltenpoth, Michael Kamp, and Jilles Vreeken. Nothing but regrets—privacy-preserving federated causal discovery. In *International Conference on Artificial Intelligence and Statistics*, pages 8263–8278. PMLR, 2023.
- [40] Luan Pham, Huong Ha, and Hongyu Zhang. Root cause analysis for microservice system based on causal inference: How far are we? In *Proceedings of the 39th IEEE/ACM International Conference on Automated Software Engineering*, pages 706–715, 2024.
- [41] Maarten G Poirot, Praneeth Vepakomma, Ken Chang, Jayashree Kalpathy-Cramer, Rajiv Gupta, and Ramesh Raskar. Split learning for collaborative deep learning in healthcare. *arXiv preprint arXiv:1912.12115*, 2019.
- [42] Sebastian Schmidl, Phillip Wenig, and Thorsten Papenbrock. Anomaly detection in time series: a comprehensive evaluation. *Proceedings of the VLDB Endowment*, 15(9):1779–1797, May 2022.
- [43] Syed Yousaf Shah, Xuan-Hong Dang, and Petros Zerfos. Root Cause Detection using Dynamic Dependency Graphs from Time Series Data. In *2018 IEEE International Conference on Big Data (Big Data)*, pages 1998–2003, December 2018.
- [44] Huasong Shan, Yuan Chen, Haifeng Liu, Yunpeng Zhang, Xiao Xiao, Xiaofeng He, Min Li, and Wei Ding. τ -diagnosis: Unsupervised and real-time diagnosis of small-window long-tail latency in large-scale microservice platforms. In *The World Wide Web Conference*, pages 3215–3222, 2019.
- [45] Hyeok-Ki Shin, Woomyo Lee, Seungoh Choi, Jeong-Han Yun, and Byung-Gi Min. Hai security datasets, 2023.

- [46] Abhishek Singh, Praneeth Vepakomma, Otkrist Gupta, and Ramesh Raskar. Detailed comparison of communication efficiency of split learning and federated learning. *arXiv preprint arXiv:1909.09145*, 2019.
- [47] Virginia Smith, Chao-Kai Chiang, Maziar Sanjabi, and Ameet S Talwalkar. Federated multi-task learning. In *Advances in Neural Information Processing Systems*, volume 30. Curran Associates, Inc., 2017.
- [48] Alex Tank, Ian Covert, Nicholas Foti, Ali Shojaie, and Emily B. Fox. Neural Granger Causality. *IEEE Transactions on Pattern Analysis and Machine Intelligence*, 44(8):4267–4279, August 2022.
- [49] Ming Tao, Kaoru Ota, and Mianxiong Dong. Locating Compromised Data Sources in IoT-Enabled Smart Cities: A Great-Alternative-Region-Based Approach. *IEEE Transactions on Industrial Informatics*, 14(6):2579–2587, June 2018.
- [50] Praneeth Vepakomma et al. Split learning for health: Distributed deep learning without sharing raw patient data. *Proceedings of the 28th International Conference on Neural Information Processing Systems*, 2018.
- [51] Guancheng Wan, Wenke Huang, and Mang Ye. Federated graph learning under domain shift with generalizable prototypes. In *Proceedings of the AAAI conference on artificial intelligence*, volume 38, pages 15429–15437, 2024.
- [52] Dongjie Wang, Zhengzhang Chen, Yanjie Fu, Yanchi Liu, and Haifeng Chen. Incremental Causal Graph Learning for Online Root Cause Analysis. In *Proceedings of the 29th ACM SIGKDD Conference on Knowledge Discovery and Data Mining*, pages 2269–2278, Long Beach CA USA, August 2023. ACM.
- [53] Dongjie Wang, Zhengzhang Chen, Jingchao Ni, Liang Tong, Zheng Wang, Yanjie Fu, and Haifeng Chen. Interdependent causal networks for root cause localization. In *Proceedings of the 29th ACM SIGKDD Conference on Knowledge Discovery and Data Mining*, KDD '23, page 5051–5060, New York, NY, USA, 2023. Association for Computing Machinery.
- [54] Ganyu Wang, Bin Gu, Qingsong Zhang, Xiang Li, Boyu Wang, and Charles X. Ling. A unified solution for privacy and communication efficiency in vertical federated learning. *Advances in Neural Information Processing Systems*, 36:13480–13491, December 2023.
- [55] Zhenggeng Ye, Shubin Si, Hui Yang, Zhiqiang Cai, and Fuli Zhou. Machine and Feedstock Interdependence Modeling for Manufacturing Networks Performance Analysis. *IEEE Transactions on Industrial Informatics*, 18(8):5067–5076, August 2022.
- [56] Qingsong Zhang, Bin Gu, Cheng Deng, and Heng Huang. Secure bilevel asynchronous vertical federated learning with backward updating. In *Proceedings of the AAAI Conference on Artificial Intelligence*, volume 35, pages 10896–10904, 2021.
- [57] Dingyi Zheng, Xiuwen Fu, Xiangwei Liu, Liudong Xing, and Rui Peng. Modeling and Analysis of Cascading Failures in Industrial Internet of Things Considering Sensing-Control Flow and Service Community. *IEEE Transactions on Reliability*, pages 1–15, 2024.

Appendices

Contents

A	Additional Results	15
A.1	Details on Synthetic Datasets	15
A.1.1	Experimental Settings	15
A.1.2	Threshold Sensitivity	16
A.2	Real World Industrial Dataset	16
A.2.1	Pre-processing Steps	16
A.2.2	Experimental Settings	16
A.2.3	Training	17
A.2.4	Inference	18
B	Proofs	19
B.1	Inferencing: Root Cause Analysis	19
B.1.1	Proposition 5.2	19
B.2	Convergence Analysis	20
B.2.1	Lemma 6.5	20
B.2.2	Proposition 6.8	21
B.2.3	Theorem 6.10	21
B.2.4	Theorem 6.13	23
B.3	Privacy Analysis	23
B.3.1	Theorem 7.1	24
B.3.2	Theorem 7.2	24
B.3.3	Theorem 7.3	24
C	Pseudocode	26
C.1	Training: Cross-Client Learning of Interdependencies	26
C.2	Inference: Root Cause Analysis	26

A Additional Results

A.1 Details on Synthetic Datasets

A.1.1 Experimental Settings

We generate synthetic data using LSTM-based state transition models, dependency functions, and measurement functions. The training (and nominal phase of inference) data generation process ensures smooth variations without abrupt anomalies, maintaining consistency with real-world settings.

The system dynamics are modeled using an LSTM-based state transition function f_m , which maps the previous state to the next state. Each client maintains an independent non-linear transition model with a hidden dimension of 16:

$$x_{t+1} = f_m(x_t), \quad (11)$$

where f_m is a single-layer LSTM followed by a fully connected layer. Interdependencies among clients are captured using an LSTM-based function g_{dep} , which models weakened dependencies for nominal data to minimize anomaly propagation. It consists of a two-layer LSTM with 64 hidden units and a fully connected layer, with a scaling factor $\alpha = 0.5$ to reduce dependency strength:

$$g_{\text{dep}}(x_t) = \alpha \cdot \tanh(W_{\text{dep}} \cdot \text{LSTM}(x_t)), \quad (12)$$

where W_{dep} is a learned transformation matrix. Observations are generated using a measurement function h_m , which maps the latent states to measurements. It consists of a two-layer feedforward network with a SELU activation in the first layer and an identity function in the second:

$$y_t = h_m(x_t) + \eta_t, \quad \eta_t \sim \mathcal{N}(0, \sigma_m^2). \quad (13)$$

A learnable scaling factor of 50 is applied to ensure comparability with anomalous data. To ensure smooth variations in nominal states, a sinusoidal target vector is generated:

$$x_t = A_t \cdot \sin\left(\frac{2\pi t}{T_s}\right) + \epsilon_t, \quad \epsilon_t \sim \mathcal{N}(0, \sigma_s^2), \quad (14)$$

where A_t represents a slowly varying step function and $T_s = 20$ is the step size. The system consists of M clients, each with P state dimensions and D measurement dimensions. At each timestep t , the root cause client updates its state using f_m . Other clients update based on both f_m and dependencies from g_{dep} . Process noise $\mathcal{N}(0, \sigma_p^2)$ is then added to simulate real-world variations. Finally Measurements are obtained through h_m , with additional measurement noise $\mathcal{N}(0, \sigma_m^2)$.

We introduce sustained anomalies into the synthetic dataset to evaluate the framework’s ability to detect and localize anomalies. The anomalous data generation follows a structured approach to ensure consistency with real-world industrial fault patterns while maintaining the statistical properties of nominal data. Anomalies are injected into the target vector using controlled perturbations:

$$x_t = A_t \cdot \sin\left(\frac{2\pi t}{T_s}\right) + \epsilon_t + \delta_t, \quad (15)$$

where, A_t represents smooth nominal variations, $\epsilon_t \sim \mathcal{N}(0, \sigma_s^2)$ is small stochastic noise, and δ_t is the anomaly term, which introduces sustained deviations. Anomalies are injected periodically every five intervals, lasting for a sustained duration of 10 timesteps. This simulates real-world scenarios where faults persist over time rather than appearing as transient spikes.

To create anomalies, a magnitude shift of $\Delta = 2.0$ is applied across all affected clients:

$$\delta_t = \begin{cases} \Delta, & \text{if } t \in \mathcal{T}_{\text{anomaly}} \\ 0, & \text{otherwise} \end{cases} \quad (16)$$

where $\mathcal{T}_{\text{anomaly}}$ represents the set of timesteps where anomalies occur. Anomalies are applied uniformly across all clients, ensuring a system-wide deviation. Each anomaly event is logged to track when and where anomalies were introduced:

$$\mathcal{A} = \{(t, m) \mid t \in \mathcal{T}_{\text{anomaly}}, m \in M\}, \quad (17)$$

where \mathcal{A} stores the affected timesteps and clients.

A.1.2 Threshold Sensitivity

In Fig. 5, we evaluate the impact of the anomaly detection threshold τ_a by varying its percentile from 75 to 97.5 and measuring its effect on ARL_0 (false alarms), ARL_1 (timely detections), and RCA (precision and recall). The results indicate that while precision and recall remain relatively stable across different τ_a values, anomaly detection performance is highly sensitive to τ_a . In particular, ARL_1 (delay in detection) exhibits an exponential increase with a higher threshold τ_a . This emphasizes the challenge of selecting an optimal τ_a and mandates further investigation.

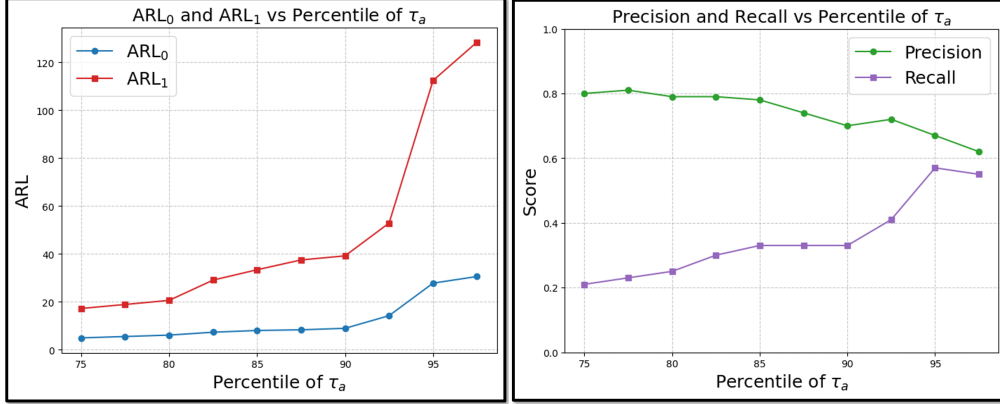


Figure 5: Sensitivity of ARL_0 , and ARL_1 (left), and Precision-Recall to threshold τ_a

A.2 Real World Industrial Dataset

The study employs the public HAI 23.05 cyber-physical system benchmark, which records physical sensor measurements like flow, level, pressure, temperature, vibration, and valve-position signals, etc., from three processes – Boiler (P1), Turbine (P2), Water Treatment (P3) along with a *Hardware-in-Loop* (HIL) simulation (P4) that introduces dependencies between P1, P2, and P3.

A.2.1 Pre-processing Steps

We retain only P1, P2, and P3, thereby removing the HIL simulation (which has only 1 sensor). Furthermore, in our study, we only utilize physical sensor measurements from P1, P2, and P3. Boolean and Integral (or %) variables arising from control valves (CV) or set points (SP) in any of P1, P2, and P3 are not considered, as they do not directly contribute to the process dynamics.

To place every variable on a common, dimensionless footing, we center its trajectory by the mean operating level and scale it by the corresponding standard deviation estimated exclusively from the training dataset. The resulting transformation parameters (μ and σ pairs) are archived separately for P1, P2, and P3, so that any future segment can be mapped into the very same standardized feature space without recalculating statistics. All training logs are first concatenated and chronologically ordered. For the test data (inference), the stored parameters are applied to every labeled test segment, ensuring normalization and preserving unaltered timestamps.

A.2.2 Experimental Settings

Train/Test Split. Models use the dataset’s official partition (nominal operation for training, attacks for testing), trained on the first 10,000 time-steps to capture dependencies while maintaining tractability.

Proprietary Client Model. Each client $c \in \{P1, P2, P3\}$ trains an EKF with LSTM state transition function f_m (width 16, $P = 2$) and MLP head based measurement function h_m (SELU, width 32), optimized via Adam ($\text{lr}=10^{-3}$, 10 epochs, $L = 20$, batch=64) on MSE. Inference uses f_m, h_m with identity-initialized covariance and $Q, R \propto I$.

Augmented Client Model. Each client adds ϕ_m (LSTM, width 1, output P) predicting $\delta_t = \phi_m(y_m^t)$ for state correction $(\hat{x}_m^t)_a \leftarrow (\hat{x}_m^t)_c + \delta_t$, updated via proprietary model loss and server gradients.

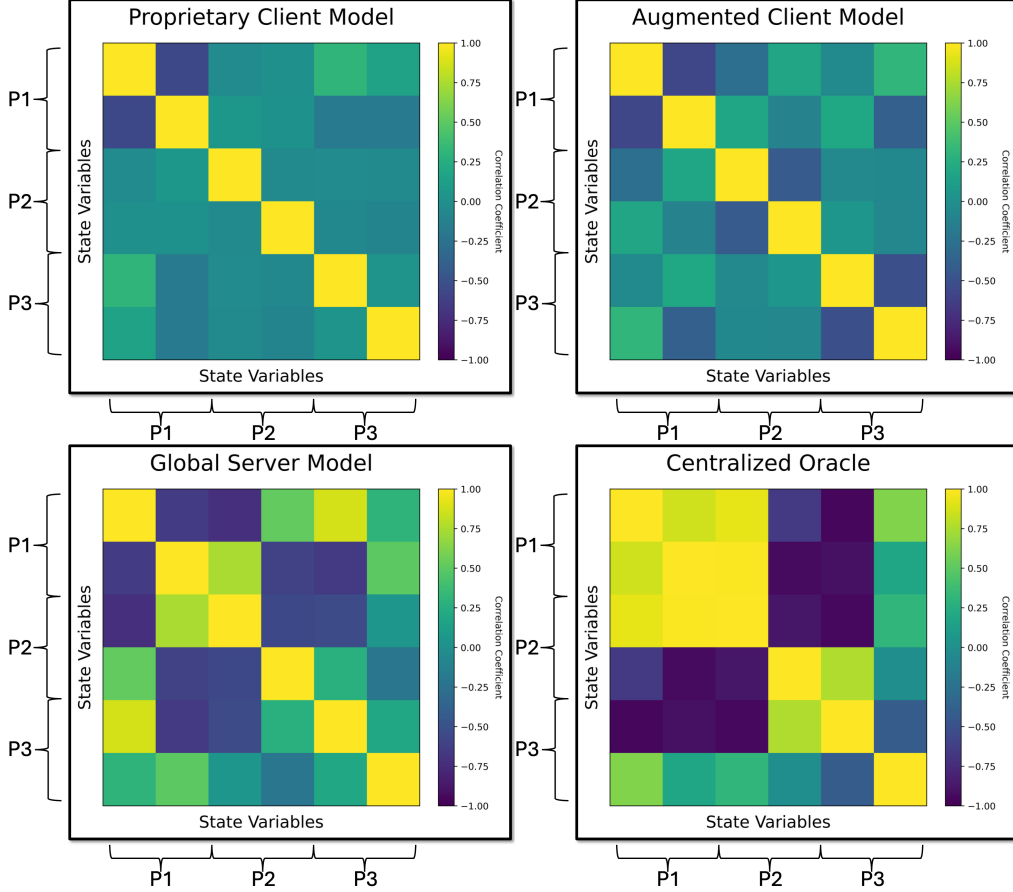


Figure 6: Correlations between the estimated states of P1, P2, and P3 in proprietary client models (top left), augmented client models (top right), global server model (bottom left), and centralized oracle (bottom right).

Global Server Model. Server LSTM f_s (width 64) maps $\mathbf{x}^{t-1} \in \mathbb{R}^{MP}$ ($M = 3, P = 2$) to predictions, updated online via Adam ($\text{lr}=10^{-3}$) with gradients $\nabla_{\hat{\mathbf{x}}_a^t} L_s$ for client updates.

Centralized Oracle. EKF that uses LSTM (width 128, $P_{\text{tot}} = 6$) for state transition func. and MLP head (SELU, width 4) for measurement func., trained with $L=20$, $\text{batch}=64$, 10 epochs, $\text{lr}=5 \times 10^{-3}$.

Hardware. PyTorch 3 on CPU-only Google Colab (13GB RAM), without dropout, or grad. clipping.

A.2.3 Training

Training on the HAI 23.05 benchmark, we quantify how well each model variant captures the real cross-process couplings among P1, P2, and P3. Fig. 6 presents the Pearson correlation matrices of the concatenated states (2 states each per process, from all 3 processes) obtained using the following four models: (1) Proprietary Client Model, (2) Augmented Client Model, (3) Global Server Model, and (4) Centralized Oracle.

The four correlation maps reveal a clear progression in the ability to capture cross-process structure. The *Proprietary Client Model*, trained in isolation, displays bright diagonal blocks but near-zero off-diagonals, signalling that it primarily encodes within-process dynamics while remaining largely blind to interdependencies between P2 and P3. Augmenting this model with a small network ϕ_m with 1 hidden layer changes this picture markedly: the augmented clients exhibit pronounced positive correlations in the P2 – P3 and P1-P2 blocks.

The iterative optimization between the client and the server sharpens the off-diagonal patterns of the *Global Server Model*, and the resulting correlation matrix becomes similar to that of the *Centralized*

Oracle. This further indicates that the joint predictor f_s successfully propagates inter-process information back to every client.

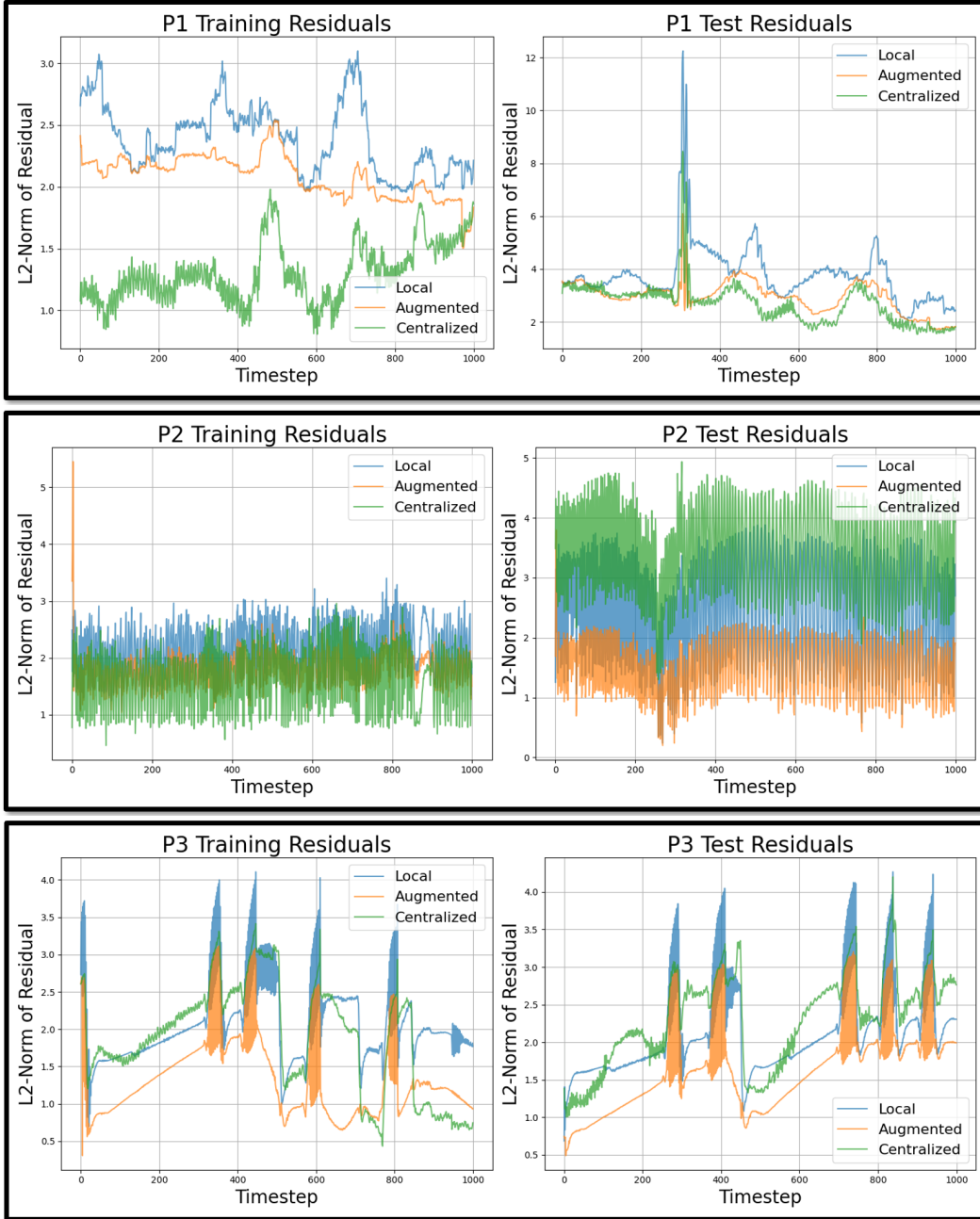


Figure 7: Training and test residuals for the first 1000 time steps in P1 (top), P2 (middle), and P3 (bottom). Each figure shows the L_2 norm of the residuals for the proprietary client model (labeled as “local”), augmented client model, and the centralized oracle.

A.2.4 Inference

Residuals. Fig. 7 presents the L_2 -norm residuals (or reconstruction error for high-dimensional data) for P1, P2, P3 over the first 1,000 time-steps in both training and test cases. In every case, for most time instants the residual curves obey the ordering, *Local (Proprietary) Client Model* > *Augmented Client Model* > *Centralized Oracle*. Dur-

Table 4: Summary of ARL_0 , ARL_1 , RCA accuracy, and RCA delay (mean \pm std) at different Mahalanobis-threshold percentiles for each modeling approach.

Percentile	Model	ARL_0 (min)	ARL_1 (min)	RCA Accuracy (%)	RCA Delay in min (mean \pm std. dev)
95%	Proprietary Client	71.00	48.50	50%	22.00 \pm 11.05
	Our Methodology	131.00	52.50		
	Centralized Oracle	89.00	52.50		
99.5%	Proprietary Client	71.00	48.50	37.5%	8.25 \pm 8.63
	Our Methodology	70.66	48.50		
	Centralized Oracle	59.66	48.50		

ing both nominal and attack conditions, the (local) proprietary client model exhibits the largest residuals while the augmented client model consistently lowers the error, approaching the centralized oracle benchmark. This ordering enables us to do systematic RCA using localized residual-based anomaly detection and ensures the validity of Table 1 (see main text of the paper).

Performance Metrics. We first infer client-specific Mahalanobis thresholds at selected training-percentile levels (95%, 99.5%), and then, for each threshold, convert every model’s residual series into a Boolean alarm flag per minute. Using these flags we compute: (i) ARL_0 , the average time to first false alarm on nominal training data; (ii) ARL_1 , over the known attack windows on test data; and (iii) RCA accuracy, and (iv) RCA delay (mean \pm std dev.).

We limit the inference experiments to *August 12, 2022*, where the details of the attack scenarios including start time and duration is provided. Furthermore, we know that the ground-truth root cause (or location of the attack) is P1. Table 4 presents the aforementioned performance metrics for the Proprietary Client Model, Our Methodology (Augmented Client Model + Global Server Model), and the Centralized Oracle, across the three percentile thresholds for the data on *August 12, 2022*.

As the Mahalanobis-threshold percentile increases from 95 % to 99.5 %, ARL_0 for all models rises showing fewer false alarms under nominal conditions. On the other hand, ARL_1 remains essentially unchanged, since every attack eventually exceeds even the strictest cutoff. Our methodology, at 95 % we observe $ARL_0 = 131$ min (versus 71 min for the proprietary client and 89 min for the oracle), perfect detection speed ($ARL_1 = 52.5$ min), but only 50 % RCA accuracy with a relatively large attribution delay of 22.0 ± 11.1 min. When we tighten to 99.5%, ARL_0 falls to 70.7 min, on par with the proprietary filter and close to the centralized benchmark (59.7 min). Furthermore, the attribution delay improves dramatically to 8.3 ± 8.6 min, albeit at the cost of lower RCA accuracy (37.5%). This trade-off shows that raising the threshold reduces false positives and speeds up root-cause analysis, but can also miss correct attributions, allowing practitioners to tune between accuracy and timeliness.

B Proofs

B.1 Inferencing: Root Cause Analysis

B.1.1 Proposition 5.2

Proof. We know that primary anomalies at each client follow a Poisson arrival process (assumption). For a single client C_m , the probability of an anomaly occurring in Δt is proportional to $\lambda_m \Delta t$, where λ_m is the Poisson rate parameter for C_m . Furthermore, the arrival processes for primary anomalies are independent across clients.

Probability of Multiple Anomalies:

- The probability of exactly one client experiencing an anomaly in Δt is:

$$P \left(\sum_{m=1}^M N_m(\Delta t) = 1 \right) = \sum_{m=1}^M \lambda_m \Delta t + \mathcal{O}(\Delta t^2).$$

- The probability of two or more clients experiencing anomalies in Δt is:

$$P\left(\sum_{m=1}^M N_m(\Delta t) > 1\right) = \mathcal{O}(\Delta t^2).$$

As $\Delta t \rightarrow 0$, the second-order term $\mathcal{O}(\Delta t^2)$ vanishes faster than the first-order term, making the probability of multiple clients experiencing anomalies negligible:

$$\lim_{\Delta t \rightarrow 0} P\left(\sum_{m=1}^M N_m(\Delta t) > 1\right) = 0.$$

□

B.2 Convergence Analysis

B.2.1 Lemma 6.5

Proof. We want to bound

$$\mathbb{E}\left\|\phi_m(y_m^{t-1}; \theta_m^k) - \sum_{n \neq m} \mathbb{E}(\hat{x}_n^{t-1})_o\right\|.$$

Adding and subtracting the term $\phi_m(y_m^{t-1}; \theta_m^*)$ inside the norm we obtain

$$\begin{aligned} & \phi_m(y_m^{t-1}; \theta_m^k) - \sum_{n \neq m} \mathbb{E}(\hat{x}_n^{t-1})_o \\ &= \underbrace{\left[\phi_m(y_m^{t-1}; \theta_m^k) - \phi_m(y_m^{t-1}; \theta_m^*)\right]}_{\text{(i)}} + \underbrace{\left[\phi_m(y_m^{t-1}; \theta_m^*) - \sum_{n \neq m} \mathbb{E}(\hat{x}_n^{t-1})_o\right]}_{\text{(ii)}}. \end{aligned}$$

By the triangle inequality,

$$\mathbb{E}\left\|\phi_m(y_m^{t-1}; \theta_m^k) - \sum_{n \neq m} \mathbb{E}(\hat{x}_n^{t-1})_o\right\| \leq \|(i)\| + \|(ii)\|.$$

Term (ii). By definition of the irreducible error (Definition 6.4),

$$\|(ii)\| = \mathbb{E}\left\|\phi_m(y_m^{t-1}; \theta_m^*) - \sum_{n \neq m} \mathbb{E}(\hat{x}_n^{t-1})_o\right\| = \epsilon^*.$$

Term (i). By the assumption that $\phi_m(\cdot; \theta_m)$ is \mathcal{L}_{θ_m} -Lipschitz in θ_m , we have

$$\mathbb{E}\left\|\phi_m(y_m^{t-1}; \theta_m^k) - \phi_m(y_m^{t-1}; \theta_m^*)\right\| \leq \mathcal{L}_{\theta_m} \|\theta_m^k - \theta_m^*\|.$$

Combining the two terms,

$$\mathbb{E}\left\|\phi_m(y_m^{t-1}; \theta_m^k) - \sum_{n \neq m} \mathbb{E}(\hat{x}_n^{t-1})_o\right\| \leq \mathcal{L}_{\theta_m} \|\theta_m^k - \theta_m^*\| + \epsilon^*.$$

Convergence. Under the assumptions that the augmented client loss $(L_m)_a$ is convex and \mathcal{L}_{L_m} -Lipschitz smooth, and with learning rates $\eta_1, \eta_2 \leq 1/L$, we have $\theta_m^k \rightarrow \theta_m^*$ as $k \rightarrow \infty$. Thus,

$$\lim_{k \rightarrow \infty} \mathbb{E}\left\|\phi_m(y_m^{t-1}; \theta_m^k) - \sum_{n \neq m} \mathbb{E}(\hat{x}_n^{t-1})_o\right\| \leq \lim_{k \rightarrow \infty} \left(\mathcal{L}_{\theta_m} \|\theta_m^k - \theta_m^*\| + \epsilon^*\right) = \epsilon^*.$$

Hence, the limit of the norm difference is bounded by ϵ^* .

□

B.2.2 Proposition 6.8

Proof. We know that the Jacobians of the state transitions for both the local client model and the centralized oracle are bounded. Let f_m represent the state transition function of client m , and f represent the state transition function of the centralized oracle.

For client m , let z_m be the input to its local state transition function, and let \mathbf{z} denote the combined state across all clients (input to the centralized oracle). The extraction function Extract_m maps the centralized state transition output to the corresponding client m 's state.

The structural difference is defined as:

$$\mathbb{E}\|f_m(z_m) - \text{Extract}_m(f(\mathbf{z}))\|.$$

Expanding $f_m(z_m)$ and $\text{Extract}_m(f(\mathbf{z}))$, we note that the boundedness of the Jacobians implies that there exist constants \mathcal{L}_{f_m} and \mathcal{L}_f , representing the Lipschitz constants of f_m and f respectively, such that:

$$\|f_m(z_m) - f_m(z'_m)\| \leq \mathcal{L}_{f_m}\|z_m - z'_m\| \quad \text{and} \quad \|f(\mathbf{z}) - f(\mathbf{z}')\| \leq \mathcal{L}_f\|\mathbf{z} - \mathbf{z}'\|.$$

Furthermore, the mapping Extract_m is linear and bounded, meaning there exists a constant C_m such that:

$$\|\text{Extract}_m(f(\mathbf{z})) - \text{Extract}_m(f(\mathbf{z}'))\| \leq C_m\|f(\mathbf{z}) - f(\mathbf{z}')\|.$$

Now, consider the difference:

$$\mathbb{E}\|f_m(z_m) - \text{Extract}_m(f(\mathbf{z}))\|.$$

Using the triangle inequality:

$$\mathbb{E}\|f_m(z_m) - \text{Extract}_m(f(\mathbf{z}))\| \leq \mathbb{E}\|f_m(z_m) - f_m(z'_m)\| + \mathbb{E}\|f_m(z'_m) - \text{Extract}_m(f(\mathbf{z}))\|.$$

By the Lipschitz property of f_m :

$$\mathbb{E}\|f_m(z_m) - f_m(z'_m)\| \leq \mathcal{L}_{f_m}\|z_m - z'_m\|.$$

For the second term, using the boundedness of Extract_m and the Lipschitz property of f :

$$\mathbb{E}\|f_m(z'_m) - \text{Extract}_m(f(\mathbf{z}))\| \leq C_m\mathcal{L}_f\|\mathbf{z} - \mathbf{z}'\|.$$

Combining these results:

$$\mathbb{E}\|f_m(z_m) - \text{Extract}_m(f(\mathbf{z}))\| \leq \mathcal{L}_{f_m}\|z_m - z'_m\| + C_m\mathcal{L}_f\|\mathbf{z} - \mathbf{z}'\|.$$

Since z_m , \mathbf{z} , and their respective transformations are bounded, there exists a constant δ_m such that:

$$\mathbb{E}\|f_m(z_m) - \text{Extract}_m(f(\mathbf{z}))\| \leq \delta_m. \quad \square$$

B.2.3 Theorem 6.10

Proof. The augmented client model predicts the state as:

$$(x_m^{t,k})_a = f_m\left(\mathbb{E}[(\hat{x}_m^{t-1})_c] + \phi_m(y_m^{t-1}; \theta_m^k)\right),$$

while the centralized oracle predicts the state using information from all clients:

$$(x_m^t)_o = f_m\left(\mathbb{E}[(\hat{x}_m^{t-1})_o], \{\mathbb{E}[(\hat{x}_n^{t-1})_o]\}_{n \neq m}\right).$$

The difference between the predicted states is:

$$(x_m^{t,k})_a - (x_m^t)_o = f_m\left(\mathbb{E}[(\hat{x}_m^{t-1})_c] + \phi_m(y_m^{t-1}; \theta_m^k)\right) - \text{Extract}_m\left(f_m\left(\mathbb{E}[(\hat{x}_m^{t-1})_o], \{\mathbb{E}[(\hat{x}_n^{t-1})_o]\}_{n \neq m}\right)\right).$$

Using the Lipschitz continuity of $f_m(\cdot)$, we have:

$$\|f_m(\mathbf{x}_1) - f_m(\mathbf{x}_2)\| \leq \mathcal{L}_{f_m} \|\mathbf{x}_1 - \mathbf{x}_2\|, \quad \forall \mathbf{x}_1, \mathbf{x}_2.$$

Substituting:

$$\mathbf{x}_1 = \mathbb{E}[(\hat{x}_m^{t-1})_c] + \phi_m(y_m^{t-1}; \theta_m^k), \quad \mathbf{x}_2 = \left(\mathbb{E}[(\hat{x}_m^{t-1})_o], \{\mathbb{E}[(\hat{x}_n^{t-1})_o]\}_{n \neq m} \right),$$

we obtain:

$$\begin{aligned} \left\| f_m \left(\mathbb{E}[(\hat{x}_m^{t-1})_c] + \phi_m(y_m^{t-1}; \theta_m^k) \right) - f_m \left(\mathbb{E}[(\hat{x}_m^{t-1})_o] + \phi_m(y_m^{t-1}; \theta_m^k) \right) \right\| &\leq \mathcal{L}_{f_m} \left(\left\| \mathbb{E}[(\hat{x}_m^{t-1})_c] - \mathbb{E}[(\hat{x}_m^{t-1})_o] \right\| \right. \\ &\quad \left. + \left\| \phi_m(y_m^{t-1}; \theta_m^k) - \sum_{n \neq m} \mathbb{E}[(\hat{x}_n^{t-1})_o] \right\| \right). \end{aligned}$$

We also know from Proposition 6.8 that:

$$\left\| f_m \left(\mathbb{E}[(\hat{x}_m^{t-1})_o] + \phi_m(y_m^{t-1}; \theta_m^k) \right) - \text{Extract}_m \left(f \left(\mathbb{E}[(\hat{x}_m^{t-1})_o], \{\mathbb{E}[(\hat{x}_n^{t-1})_o]\}_{n \neq m} \right) \right) \right\| \leq \delta_m.$$

Thus, we obtain the following upper bound:

$$\left\| (x_m^{t,k})_a - (x_m^t)_o \right\| \leq \mathcal{L}_{f_m} \left(\left\| \mathbb{E}[(\hat{x}_m^{t-1})_c] - \mathbb{E}[(\hat{x}_m^{t-1})_o] \right\| + \left\| \phi_m(y_m^{t-1}; \theta_m^k) - \sum_{n \neq m} \mathbb{E}[(\hat{x}_n^{t-1})_o] \right\| \right) + \delta_m.$$

Next, we apply Lemma 6.5. Recall:

$$\left\| \phi_m(y_m^{t-1}; \theta_m^k) - \sum_{n \neq m} \mathbb{E}[(\hat{x}_n^{t-1})_o] \right\| \leq \mathcal{L}_{\theta_m} \|\theta_m^k - \theta_m^*\| + \epsilon^*,$$

where ϵ^* is the irreducible error. Substituting the lemma into the first inequality, we have:

$$\left\| (x_m^{t,k})_a - (x_m^t)_o \right\| \leq \mathcal{L}_{f_m} \left(\left\| \mathbb{E}[(\hat{x}_m^{t-1})_c] - \mathbb{E}[(\hat{x}_m^{t-1})_o] \right\| + \mathcal{L}_{\theta_m} \|\theta_m^k - \theta_m^*\| + \epsilon^* \right) + \delta_m.$$

Focusing on $\left\| \mathbb{E}[(\hat{x}_m^t)_c] - \mathbb{E}[(\hat{x}_m^t)_o] \right\|$, and using the structure of the Kalman filter estimates and the Lipschitz continuity of $h_m(\cdot)$, we derive the recursion:

$$D_t := \left\| \mathbb{E}[(\hat{x}_m^t)_c] - \mathbb{E}[(\hat{x}_m^t)_o] \right\| \leq \|\Delta K_m\| \cdot \mathbb{E}[\|(r_m^t)_o\|] + \mathcal{L}_{h_m} C_x + (1 + \|\Delta K_m\| \mathcal{L}_{h_m}) \left(\mathcal{L}_{f_m} D_{t-1} + \mathcal{L}_{f_m} (M-1) C_x \right),$$

where $(r_m^t)_o := y_m^t - h_m((x_m^t)_o)$.

Expanding the recursion iteratively and assuming the stability condition $1 + \|\Delta K_m\| \mathcal{L}_{h_m} < \frac{1}{\mathcal{L}_{f_m}}$, the recursive terms decay geometrically. The steady-state error D_t is bounded by:

$$\lim_{t \rightarrow \infty} D_t \leq \frac{\|\Delta K_m\| \sup_t \mathbb{E}[\|(r_m^t)_o\|] + \mathcal{L}_{h_m} C_x + \mathcal{L}_{f_m} (M-1) C_x}{1 - (1 + \|\Delta K_m\| \mathcal{L}_{h_m}) \mathcal{L}_{f_m}}.$$

Substituting this result into the bound for $\left\| (x_m^{t,k})_a - (x_m^t)_o \right\|$, and noting that $\|\theta_m^k - \theta_m^*\| \rightarrow 0$ as $k \rightarrow \infty$, we obtain:

$$\lim_{k \rightarrow \infty} \left\| (x_m^{t,k})_a - (x_m^t)_o \right\| \leq \mathcal{L}_{f_m} \left(\rho + \epsilon^* \right) + \delta_m,$$

where:

$$\rho := \frac{\|\Delta K_m\| \sup_t \mathbb{E}[\|(r_m^t)_o\|] + \mathcal{L}_{h_m} C_x + \mathcal{L}_{f_m} (M-1) C_x}{1 - (1 + \|\Delta K_m\| \mathcal{L}_{h_m}) \mathcal{L}_{f_m}}.$$

Thus, the error converges as claimed. \square

B.2.4 Theorem 6.13

Proof. We aim to bound the error $\mathbb{E}[\|x_s^{t,k} - x_o^t\|]$, where:

$$x_s^{t,k} = f_s(\{\mathbb{E}[(\hat{x}_m^t)_c]\}_{m=1}^M; \theta_s^k), \quad x_o^t = f(\{\mathbb{E}[(\hat{x}_m^t)_o]\}_{m=1}^M).$$

Re-writing the difference, we obtain:

$$\|x_s^{t,k} - x_o^t\| = \|f_s(\{\mathbb{E}[(\hat{x}_m^t)_c]\}_{m=1}^M; \theta_s^k) - f_s(\{\mathbb{E}[(\hat{x}_m^t)_o]\}_{m=1}^M; \theta_s^k) + f_s(\{\mathbb{E}[(\hat{x}_m^t)_o]\}_{m=1}^M; \theta_s^k) - f(\{\mathbb{E}[(\hat{x}_m^t)_o]\}_{m=1}^M)\|.$$

Using the triangle inequality, this is bounded as:

$$\|x_s^{t,k} - x_o^t\| \leq \|f_s(\{\mathbb{E}[(\hat{x}_m^t)_c]\}_{m=1}^M; \theta_s^k) - f_s(\{\mathbb{E}[(\hat{x}_m^t)_o]\}_{m=1}^M; \theta_s^k)\| + \|f_s(\{\mathbb{E}[(\hat{x}_m^t)_o]\}_{m=1}^M; \theta_s^k) - f(\{\mathbb{E}[(\hat{x}_m^t)_o]\}_{m=1}^M)\|.$$

Using Lipschitz continuity of f_s with respect to its inputs, with constant \mathcal{L}_{f_s} , we have:

$$\|f_s(\{\mathbb{E}[(\hat{x}_m^t)_c]\}_{m=1}^M; \theta_s^k) - f_s(\{\mathbb{E}[(\hat{x}_m^t)_o]\}_{m=1}^M; \theta_s^k)\| \leq \mathcal{L}_{f_s} \sum_{m=1}^M \|\mathbb{E}[(\hat{x}_m^t)_c] - \mathbb{E}[(\hat{x}_m^t)_o]\|.$$

Let $D_t := \|\mathbb{E}[(\hat{x}_m^t)_c] - \mathbb{E}[(\hat{x}_m^t)_o]\|$. Then:

$$\|f_s(\{\mathbb{E}[(\hat{x}_m^t)_c]\}_{m=1}^M; \theta_s^k) - f_s(\{\mathbb{E}[(\hat{x}_m^t)_o]\}_{m=1}^M; \theta_s^k)\| \leq \mathcal{L}_{f_s} \cdot M \cdot \sup_m D_t.$$

In the steady state (large t), using Theorem 6.10, D_t satisfies:

$$D_t \leq \frac{\|\Delta K_m\| \sup_t \mathbb{E}[\|(r_m^t)_o\|] + \mathcal{L}_{h_m} C_x + \mathcal{L}_{f_m} (M-1) C_x}{1 - (1 + \|\Delta K_m\| \mathcal{L}_{h_m}) \mathcal{L}_{f_m}}.$$

Using Definition 6.11:

$$\lim_{k \rightarrow \infty} \|f_s(\{\mathbb{E}[(\hat{x}_m^t)_o]\}_{m=1}^M; \theta_s^k) - f(\{\mathbb{E}[(\hat{x}_m^t)_o]\}_{m=1}^M)\| = \sigma^*.$$

Substituting:

$$\lim_{k \rightarrow \infty} \mathbb{E}[\|x_s^{t,k} - x_o^t\|] \leq \mathcal{L}_{f_s} \cdot M \cdot \rho + \sigma^*,$$

where:

$$\rho := \frac{\|\Delta K_m\| \sup_t \mathbb{E}[\|(r_m^t)_o\|] + \mathcal{L}_{h_m} C_x + \mathcal{L}_{f_m} (M-1) C_x}{1 - (1 + \|\Delta K_m\| \mathcal{L}_{h_m}) \mathcal{L}_{f_m}}.$$

□

B.3 Privacy Analysis

We provide two definitions that will be used to prove Theorems 7.1 and 7.2.

Definition B.1 (ℓ_2 -Sensitivity). The ℓ_2 -sensitivity Δ of a function $f : \mathcal{D} \rightarrow \mathbb{R}^k$ is the maximum change in the output's ℓ_2 -norm due to a change in a single data point:

$$\Delta = \max_{D, D'} \|f(D) - f(D')\|_2,$$

where D and D' are neighboring datasets.

Definition B.2 (Gaussian Mechanism). Given a function $f : \mathcal{D} \rightarrow \mathbb{R}^k$ with ℓ_2 -sensitivity Δ , the Gaussian mechanism \mathcal{M} adds noise drawn from a Gaussian distribution to each output component:

$$\mathcal{M}(D) = f(D) + \mathcal{N}(0, \sigma^2 I_k),$$

where $\sigma \geq \frac{\Delta \sqrt{2 \ln(1.25/\delta)}}{\epsilon}$ ensures that \mathcal{M} satisfies (ϵ, δ) -differential privacy.

B.3.1 Theorem 7.1

The local and augmented states are perturbed as:

$$(\tilde{x}_m^{t-1})_c = (\hat{x}_m^{t-1})_c + \mathcal{N}(0, \sigma_c^2), \quad (\tilde{x}_m^t)_a = (x_m^t)_a + \mathcal{N}(0, \sigma_a^2).$$

Substituting the Extended Kalman Filter equations, the local state estimate $(\hat{x}_m^{t-1})_c$ is:

$$(\hat{x}_m^{t-1})_c = f_m((\hat{x}_m^{t-2})_c) + K_m^c(y_m^{t-1} - h_m((\hat{x}_m^{t-1})_c)).$$

Adding bounds on the Kalman gain K_m^c and observation Jacobian H_m , the sensitivity is:

$$\Delta_c \leq \|\Delta K_m\|(\mathcal{L}_{h_m} C_x + \sup_t \|r_m^t\|),$$

where \mathcal{L}_{h_m} and C_x are bounds on h_m and state space, respectively, and r_m^t is the residual.

Similarly, substituting the augmented state equation:

$$(x_m^t)_a = f_m((\hat{x}_m^{t-1})_a) + \phi_m(y_m^t; \theta_m),$$

and bounding f_m and ϕ_m , we obtain:

$$\Delta_a \leq \mathcal{L}_{f_m} C_x + \mathcal{L}_{\theta_m} \sup_t \|y_m^t\|.$$

Adding Gaussian noise ensures (ε, δ) -differential privacy. Substituting the sensitivity terms into the noise scale equation:

$$\sigma_c \geq \frac{2\|\Delta K_m\|(\mathcal{L}_{h_m} C_x + \sup_t \|r_m^t\|)\sqrt{2\ln(1.25/\delta_c)}}{\varepsilon_c}, \quad \sigma_a \geq \frac{2(\mathcal{L}_{f_m} C_x + \mathcal{L}_{\theta_m} \sup_t \|y_m^t\|)\sqrt{2\ln(1.25/\delta_a)}}{\varepsilon_a}.$$

Adding the privacy budgets of the two mechanisms yields:

$$\varepsilon = \varepsilon_c + \varepsilon_a, \quad \delta = \delta_c + \delta_a.$$

B.3.2 Theorem 7.2

The server sends perturbed gradients:

$$\tilde{g}_m^t = \text{clip}(g_m^t, C_g) + \mathcal{N}(0, \sigma_g^2),$$

where $\text{clip}(g_m^t, C_g)$ ensures $\|g_m^t\|_2 \leq C_g$.

Substituting the gradient equation:

$$g_m^t = \nabla_{\theta_m^k} L_s = (\nabla_{(\hat{x}_m^t)_a} L_s) \cdot (\nabla_{\theta_m^k} (\hat{x}_m^t)_a),$$

and bounding each term, we find that the sensitivity is:

$$\Delta_g = \max_t \|\text{clip}(g_m^t, C_g)\|_2 \leq C_g.$$

Adding Gaussian noise ensures (ε, δ) -differential privacy. Substituting the sensitivity bound:

$$\sigma_g \geq \frac{2C_g\sqrt{2\ln(1.25/\delta)}}{\varepsilon}.$$

B.3.3 Theorem 7.3

To demonstrate that adding p_c and p_a satisfies ε -differential privacy, we analyze the randomized response mechanism as follows:

Starting with the perturbation mechanism, the binary anomaly flags are perturbed independently using:

$$\tilde{Z}_c^t = \begin{cases} Z_c^t, & \text{with probability } p_c, \\ 1 - Z_c^t, & \text{with probability } 1 - p_c, \end{cases} \quad \tilde{Z}_a^t = \begin{cases} Z_a^t, & \text{with probability } p_a, \\ 1 - Z_a^t, & \text{with probability } 1 - p_a. \end{cases}$$

Substituting the definition of ε -differential privacy, the mechanism satisfies differential if, for any two neighboring datasets \mathcal{D} and \mathcal{D}' differing in one binary flag, and any possible output \tilde{z} :

$$\frac{\Pr[\mathcal{M}(\mathcal{D}) = \tilde{z}]}{\Pr[\mathcal{M}(\mathcal{D}') = \tilde{z}]} \leq e^\varepsilon.$$

Considering the sensitivity of binary flags, the maximum difference in output caused by changing one record is:

$$\Delta_Z = \max_{Z, Z'} |Z - Z'| = 1.$$

Analyzing the probabilities of reporting $\tilde{Z}_c^t = 1$ under two neighboring datasets:

$$\Pr[\tilde{Z}_c^t = 1 \mid Z_c^t = 1] = p_c, \quad \Pr[\tilde{Z}_c^t = 1 \mid Z_c^t = 0] = 1 - p_c.$$

Dividing these probabilities, the ratio is:

$$\frac{\Pr[\tilde{Z}_c^t = 1 \mid Z_c^t = 1]}{\Pr[\tilde{Z}_c^t = 1 \mid Z_c^t = 0]} = \frac{p_c}{1 - p_c}.$$

Substituting the privacy constraint $\frac{p_c}{1 - p_c} \leq e^{\varepsilon_c}$, solving for p_c :

$$p_c = \frac{e^{\varepsilon_c}}{1 + e^{\varepsilon_c}}.$$

Similarly, analyzing the probabilities of reporting $\tilde{Z}_a^t = 1$:

$$\Pr[\tilde{Z}_a^t = 1 \mid Z_a^t = 1] = p_a, \quad \Pr[\tilde{Z}_a^t = 1 \mid Z_a^t = 0] = 1 - p_a,$$

and substituting $\frac{p_a}{1 - p_a} \leq e^{\varepsilon_a}$, solving for p_a :

$$p_a = \frac{e^{\varepsilon_a}}{1 + e^{\varepsilon_a}}.$$

Adding the privacy budgets of \tilde{Z}_c^t and \tilde{Z}_a^t , the total privacy budget is:

$$\varepsilon = \varepsilon_c + \varepsilon_a.$$

Hence, the randomized response mechanism with probabilities p_c and p_a satisfies ε -differential privacy.

C Pseudocode

C.1 Training: Cross-Client Learning of Interdependencies

Algorithm 1 Training: Federated Learning of Cross-Client Interdependencies

- 1: **Input:** Local data $y_m^{1:T}$, functions $f_m, h_m \forall m \in \{1, \dots, M\}$, learning rates η_1, η_2, η_3 .
 - 2: **Output:** Updated parameters $\theta_s, \{\theta_m\}_{m=1}^M$.
 - 3: **for** $t = 1 : T$ **do**
 - 4: **for** each *client* m **in parallel do**
 - 5: Compute augmented states $(\hat{x}_m^t)_a$ and $(x_m^t)_a$.
 - 6: Send $(\hat{x}_m^{t-1})_c$ and $(x_m^t)_a$ to the server.
 - 7: **end for**
 - 8: Server updates θ_s using $\nabla_{\theta_s^k}(L_s)$.
 - 9: Server sends $\nabla_{(x_m^t)_a}(L_s)$ to each client.
 - 10: **for** each *client* m **in parallel do**
 - 11: Update θ_m using $\nabla_{\theta_m^k}(L_m)_c$ and $\nabla_{\theta_m^k}(L_s)$.
 - 12: **end for**
 - 13: **end for**
-

C.2 Inference: Root Cause Analysis

Algorithm 2 Inference: Federated Root Cause Analysis

- 1: **Input:** Residuals r_c^t, r_a^t , thresholds τ_c, τ_a
 - 2: **Output:** Root cause and propagated effect; causal network
 - 3: **for** each *client* m **in parallel do**
 - 4: Compute Mahalanobis distances $d_{M,c}^2, d_{M,a}^2$.
 - 5: Generate anomaly flags: $Z_c^t = \mathcal{I}[d_{M,c}^2 > \tau_c], Z_a^t = \mathcal{I}[d_{M,a}^2 > \tau_a]$ where \mathcal{I} is indicator function.
 - 6: Transmit (Z_c^t, Z_a^t) to the server.
 - 7: **end for**
 - 8: *Server:* Use look-up Table 1 to identify clients with root cause and propagated effects of anomaly
-